

RESEARCH ARTICLE

Preparation of low-density high-performance porous aramid films using porosity promoter polymers

Andrea Rubio-Aguinaga  | José Antonio Reglero-Ruiz  | Asunción Muñoz  | Félix C. García  | José M. García  | Miriam Trigo-López 

Departamento de Química, Facultad de Ciencias, Universidad de Burgos, Burgos, Spain

Correspondence

Miriam Trigo-López, Departamento de Química, Facultad de Ciencias, Universidad de Burgos, Plaza de Misael Bañuelos s/n, 09001 Burgos, Spain.
Email: mtrigo@ubu.es

Funding information

Regional Government of Castilla y León (Junta de Castilla y León), the Ministry of Science and Innovation MICIN and the European Union NextGenerationEU / PRTR, and the Spanish Agencia Estatal de Investigación (State Research Agency), Grant/Award Number: PID2019-108583RJ-I00/AEI/10.13039/501100011033

Abstract

Low-density porous aramid films using inexpensive and widely available polymers as porosity promoters, that is, polyvinyl alcohol (PVA), poly(2-ethyl-2-oxazoline) (PEOx), and cellulose polyacetate (CA) were fabricated. Porous poly (*m*-phenylene isophthalamide) films were obtained by the standard casting procedure using mixtures of the aramid with either PVA, PEOx, or CA, followed by the removal of the porosity promoter polymers by immersing them in water or acetone. As a result, films with up to a 65% density reduction with pore sizes ranging from 0.02 to 10 μm and up to 30% increment in Young's modulus were obtained. In addition, the morphology of the films was homogeneous and was controlled by the proportion and nature of the porosity promoter polymer. The density reduction of materials plays a significant role in energy crises and the need for fuel reduction. This study revealed that it is possible to prepare low-density porous aramid films inexpensively without impairing their outstanding performance by using PVA in the casting procedure as a porosity promoter polymer.

KEYWORDS

films, mechanical propert, porous materials

1 | INTRODUCTION

The study and control of the relationship between the structure and the properties of materials enable the development of advanced and lighter polymers with specific properties and characteristics, which satisfy the needs of technological developments. In this sense, porous or cellular polymers stand out for their lower density while maintaining the properties of the dense materials or even showing improved characteristics. Moreover, surface area, pore size, volume and morphology, reactivity, and functionality of the polymers can be tuned depending on their end-use application,

which broadens their applications in many fields.^{1–5} However, great control of the morphology and pore size (microporous [pore size ≤ 2 nm], mesoporous [2–50 nm], and macroporous [> 50 nm]) is needed, and research efforts are directed toward the fabrication of these materials at an industrial scale.⁶

Regarding the production of porous polymeric membranes and films, the most commonly used techniques for porous membrane fabrication are based on phase inversion, for being easy and fast.⁷ Table 1 summarizes the advantages and disadvantages of traditional techniques and some other novel technologies.

This is an open access article under the terms of the [Creative Commons Attribution](https://creativecommons.org/licenses/by/4.0/) License, which permits use, distribution and reproduction in any medium, provided the original work is properly cited.

© 2022 The Authors. *Journal of Applied Polymer Science* published by Wiley Periodicals LLC.

TABLE 1 Porous polymeric membranes preparation methods

| Method | Pore formation mechanism | Advantages | Disadvantages |
|---|---|--|--|
| Vapor induced phase separation ⁸ | Gas inflow and solvent outflow transfer at the interface. | Enable the tuning of both flat-sheet and hollow-fiber polymer membranes. | Difficult to scale-up and commercialize. |
| Non-solvent induced phase separation ⁹ | Liquid–liquid phase demixing. | Allows the control of the surface and the size of the pores using additives. | A precise control of the process is difficult to achieve. |
| Thermally induced phase separation ^{10,11} | The removal of the diluent produces micropores in its previously occupied sites. | Suitable for a number of polymers. Reproducible and less susceptible to defects than other methods. | Hard to tune the surface pores. Expensive, non-environmentally friendly. |
| Phase separation micromolding ¹² | Polymer phase separation. | Possibility of sub-micrometer structures preparation and surfaces with two-tier hierarchical structures. | Limited processing and production capacity. Difficult to control de number and size of open pores. |
| Pore formers ⁶ | Removal of low molecular weight salts or polymers in a solvent. | Functionality, reactivity, surface area, pore volume, pore size and porosity of a polymer can be tailored. | Crease formation. |
| Electrospinning ¹³ | Evaporation of the solvent. | Simple and inexpensive. Uniform pore size distribution. | Low reproducibility and limited production capacity. |
| Melt-spinning and cold stretching ¹⁴ | Mechanical forces on the membrane due to cold-stretching steps. | Simple and inexpensive. No need of solvent or additives. High mechanical performance. | Low tear resistance in the transverse direction due to high orientation. |
| Sintering ⁷ | High temperature induced sintering transformation. | Widely used for inorganic and some polymeric membranes. | Expensive, materials and phase stability limitations. |
| Track etching ¹⁵ | Tracks in the membranes and pore formation by chemical etching are produced by irradiation. | Precise control of the pore sizes, shapes, and density. | Expensive and limited use and large-scale applications. |
| Imprinting / soft molding ¹⁶ | Molding with pressure. | Uniform and tunable porous structures. | Not suitable for large nano porous membrane areas. |
| 3D printing ¹⁷ | Printing an acrylate based mold and using it as a template. | Preparation of almost any shape in a range of materials at different scales. | Limited resolution and printing materials availability. High cost. |

Among polymers, aramids (aromatic polyamides) are exceptional materials for their thermal and mechanical properties combined with lower density compared to other inorganic fibers, ceramics, metals, and even carbon fibers. They are considered high-performance materials, and thus they are used for advanced applications in protective clothing and the aeronautic and automotive industries. Commercial aramids include poly(*m*-phenylene isophthalamide) (MPIA) (tradenames: Nomex[®], Teijinconex[®], and ARAWIN[®]) and poly(*p*-phenylene terephthalamide) (PPTA) (tradenames: Kevlar[®] and Twaron[®]).¹⁸ Due to their outstanding thermal stability, high cohesive energy, and low CO₂ absorption, aramids are not easily foamed, so this possibility is barely explored. Nevertheless, to further lower the density of these materials, in previous work, we were able

to prepare microporous *m*-aramids for the first time by foaming them with ScCO₂ using ionic liquids as CO₂ absorption agents, considerably reducing the density of laboratory-synthesized aramids up to 75%.¹⁹ However, the preparation of porous materials using ScCO₂ involves special experimental conditions, long processing times, and high-pressure reactors, making this procedure difficult to be implemented on an industrial scale.²⁰ Later, we demonstrated that it is possible to generate porous structures in *m*-aramid films by adding ionic liquids in the cast solution of the aramid and, after the solvent is evaporated, removing the ionic liquid by washing them with water.^{21,22} Ionic liquids are commonly used as compatibilizers in composites or solvents.^{23,24} They are highly compatible with aramids, but they are difficult to handle due to their viscosity and

hygroscopic nature,²⁵ and they are very expensive to be used at an industrial level.²⁶

In a step forward in exploring aramid porosity promoters that are cheap, effective, and can be used at a larger scale, we came to the idea of using various water or acetone soluble, inexpensive, aramid compatible polymers as an alternative for the ionic liquids. In this sense, an extensive review summarizes the use of different water-soluble polymers as pore formers to prepare different porous polymer membranes.⁶ However, for the preparation of porous aramids, only one reference was found, using *p*-aramid nanofibers and poly(ethylene glycol) (PEG) to prepare hierarchical porous nanofibrous membranes through a phase inversion procedure.²⁷ To further explore the preparation of porous aramids, we selected poly(vinyl alcohol) (PVA), poly(2-ethyl-2-oxazoline) (PEOx), and cellulose polyacetate (CA) of different molecular weights to prepare porous poly(*m*-phenylene isophthalamide) films by a casting procedure. All these polymers are innocuous and biocompatible, soluble in water or acetone, widely available, and their price is very low.^{28–32} PVA possesses a number of hydroxyl groups in its structure, as well as CA, providing many interactive sites to form hydrogen bonds with amide groups in aramids.^{33,34} PEOx is a tertiary polyamide, and it has been widely studied since it shows similar hydrophilicity to PEG and balanced amphiphilicity, demonstrating potential applications in tissue regeneration and drug delivery systems.³⁵

As previously pointed out, the objective of this work is to prepare porous poly(*m*-phenylene isophthalamide) films using these polymers as porosity promoters in an inexpensive and simple way without impairing their performance, establishing relationships between the porosity former and the properties of the films. The obtention of porous high-performance polymers with controlled pore morphology and outstanding properties plays a key role in the development of separators for ion lithium batteries,^{36–40} or osmosis membranes.^{41–43} In addition, due to their properties and low density, they are promising materials for the transport and aerospace industries, especially considering the ongoing global energy crisis and the need for fuel reduction. Also, they could expand their fields of application in biomolecules immobilization, and in heat-protective equipment to limit heat diffusion without compromising structural function.

2 | MATERIALS AND METHODS

2.1 | Materials

All materials used in this work are commercially available and were used as received: *N,N*-dimethylacetamide (DMA, Sigma-Aldrich, >99%), LiCl (Sigma-Aldrich, ≥99%),

polyvinyl alcohol (PVA) (Applichem, 85–89% wt, 10 KDa), poly(2-ethyl-2-oxazoline) (PEOx) (ThermoFisher, 50 KDa), cellulose acetate (CA) (Sigma-Aldrich, 40% wt. acetylated, 30 KDa). *meta*-aramid fiber ARAWIN[®] (PA) (nonwoven regular staple fiber of average length 6.4 mm) was supplied by Toray Advanced Materials, Inc. (Korea).

2.2 | Methods

SEM micrographs were recorded with a Scanning Electronic Microscope (JEOL JSM-6460LV). Films were fractured after freezing in liquid nitrogen and coated with gold in vacuum to provide electrical conductivity. SEM micrographs of one of the samples were also recorded using a ZEISS GeminiSEM 560 equipment.

ImageJ[®] software was used to characterize the cellular structure of the films, establishing the average bubble radius \bar{R} and average cell density by counting the number of cells (n_i) from each SEM micrograph and its radius (R_i),⁴⁴ and using Equation (1):

$$\bar{R} = \frac{\sum_{i=1}^N n_i R_i}{\sum_{i=1}^N n_i} \quad (1)$$

Cell density, (number of cells per cm³, N_C) is estimated using Kumar approximation (Equation 2) and the micrograph area (A):

$$N_C = \left(\frac{n}{A}\right)^{3/2} \quad (2)$$

Films density of the films (ρ_d) was calculated from the dimensions and weight of the samples. The film's width was measured using a digital micrometer (Sonline 25 mm/0.001 mm), taking five measurements and averaging the results.

The density of porous films (ρ_p) is estimated from SEM images using ImageJ[®] software, according to Equations (3) and (4), where V_f is defined as the gas fraction per volume and \bar{d} is the average diameter of the pore.

$$V_f = \frac{\pi \bar{d}^3 N_c}{6} \quad (3)$$

$$\rho_p = (1 - V_f) \rho_d \quad (4)$$

Atomic force microscopy (AFM) images were obtained at room temperature from film samples with a confocal

(AFM-RAMAN) model Alpha300R–Alpha300A from WITec, using an AFM tip of 42 N/m and the *tapping* mode. A 532 nm wavelength laser was used for the RAMAN spectra, working at 2 mW.

The thermogravimetric analysis was conducted on a TA instrument Q50 TGA analyzer using both air and nitrogen atmosphere. First, film samples were heated from room temperature to 100°C at 10°C/min. Then, they were kept at that temperature for 15 min to remove any moisture content. The samples were then heated at 10°C/min up to 800°C to complete the TGA analysis.

Differential scanning calorimetry (DSC) measurements were carried out using the film samples and a DSC Q200 TA Instruments equipment. The analysis was conducted by heating the samples from room temperature to 90°C at 15°C/min. The temperature was maintained 30 min to remove moisture from the films. The samples were then cooled to 30°C at 20°C/min and heated to 300°C at 15°C/min.

^1H NMR spectra were acquired using a Bruker Avance III HD spectrometer operating at 300 MHz at 25°C. Dimethyl sulfoxide ($\text{DMSO-}d_6$) was used as the solvent. Infrared spectra (FTIR) were collected with an FT/IR-4200 FT-IR Jasco Spectrometer with an ATR-PRO410-S single reflection accessory.

The mechanical performance evaluation was conducted using 5 x 40 mm strips cut from the aramid film and dried for 24 h at 80°C to remove the moisture content. Then tensile tests were conducted using a SHIMADZU EZ Test Compact Table-Top Universal Tester and mechanical clamps. A gauge length of 9.44 mm was used, with an extension rate of 5 mm/min. At least five strips of each film were tested, and the results were then averaged.

Thermal conductivity measurements were performed using a HOT-DISK TPS 2500S equipment with a radius sensor of 7.854 mm. The measurements were performed on 4 cm diameter film discs, with a measuring time of 20 s, a 0.5 W heating power and performing three replicates of each film measurement and then averaging the results.

2.3 | Preparation of dense and porous films

Films were prepared using the standard solution casting method. First, a solution containing DMA (7 ml) as the solvent, commercial poly (*m*-phenylene isophthalamide) (PA) (0.49 g) and LiCl (0.14 g, used as solubility promoter), from now on DMA/PA/LiCl, was prepared by heating the mixture at 80°C until complete dissolution is observed. The corresponding amount of porosity

promoter polymer (PPP) (PVA, PEOx or CA) was then added to the mixture at 80°C and stirred to complete their dissolution for at least 1 h. After that, the solution was poured into a glass and kept in an air-circulating oven at 80°C for 24 h to remove the DMA.

In order to remove the PPPs and generate the cellular structure, the dense films prepared were washed by immersing them in distilled water at 80°C for at least 12 h and replacing the solvent four times or by Soxhlet extraction with acetone for 24 h to ensure the complete washing. Washing was continued until the constant weight of the samples after drying in an air-circulating oven.

The properties of the films were evaluated before and after the removal of the PPPs, and the results were compared to dense aramid films prepared in the same manner (but without the porosity promoter polymer). Three samples of each film were prepared to evidence the reproducibility of the method by comparing their properties and porous structures.

3 | RESULTS AND DISCUSSION

3.1 | Preparation of dense and porous films

To define the molecular weight and nature of the PPPs, preliminary tests were carried out. Aramid films prepared as described in Section 2.3. containing PVA, PEOx or CA in different proportions as porosity promoters were tested.

PVA, PEOx, and CA load percentages were decided after conducting a solubility study for each polymer in the DMA/PA/LiCl mixture at 80°C. This way, PVA and CA are no longer soluble in the solution at weight percentages above 50%, where turbidity is observed. For PEOx, loading percentages up to 200% weight led to homogenous solutions and manageable films, while percentages over 200% rendered films with poor mechanical properties.

To evaluate the influence of the PPP (PVA, PEOx, and CA) on the morphology and the properties of the porous aramid films obtained, we prepared 17 dense films according to the procedure described in Section 2.3 of this work. For that, we kept the amount of DMA (7 ml), PA (0.49 g), and LiCl (0.14 g) constant and varied the weight percent of the porosity promoter polymer as described in Table 2.

To evaluate the distribution of the components of the films before removing the PPP, we characterized them using AFM-Raman spectroscopy. First, single components Raman spectra were collected and compared

TABLE 2 Materials and quantities used for the preparation of dense films

| Film ^a | Porosity promoter polymer (wt%) | PVA (mg) | Cellulose acetate (mg) | Poly(2-ethyl-2-oxazoline) (mg) |
|-------------------|---------------------------------|----------|------------------------|--------------------------------|
| PA | 0 | - | - | - |
| PA-PVA1 | 1 | 4.9 | - | - |
| PA-PVA5 | 5 | 24.5 | - | - |
| PA-PVA10 | 10 | 49.0 | - | - |
| PA-PVA25 | 25 | 122.5 | - | - |
| PA-CA1 | 1 | - | 4.9 | - |
| PA-CA5 | 5 | - | 24.5 | - |
| PA-CA10 | 10 | - | 49.0 | - |
| PA-CA25 | 25 | - | 122.5 | - |
| PA-CA50 | 50 | - | 245.0 | - |
| PA-PEOx1 | 1 | - | - | 4.9 |
| PA-PEOx5 | 5 | - | - | 24.5 |
| PA-PEOx10 | 10 | - | - | 49.0 |
| PA-PEOx25 | 25 | - | - | 122.5 |
| PA-PEOx50 | 50 | - | - | 245.0 |
| PA-PEOx100 | 100 | - | - | 490.0 |
| PA-PEOx200 | 200 | - | - | 980.0 |

^aAll of the solutions used to prepare the films also contain DMA (7 ml), commercial *m*-aramid (PA) (490 mg) and LiCl (140 mg).

(Figure 1). Also, the AFM-Raman spectra of the films were collected and correlated with the components of the mixture (PA in red and the PPP in blue) and used to show the distribution of the components along 17 x 17 μm film's surface. Figure 1b shows the Raman spectra of a PA film and the CA used as PPP. Two phases can be observed for this film, consisting of the PA matrix with CA aggregates. This fact is also observed for the film containing PVA (Figure 1a), although smaller aggregates are formed this time, considering that the amount of PVA with respect to the aramid is lower than when using CA. On the other hand, if PEOx is used as PPP (Figure 1c), a more homogeneous distribution is observed, which explains the fact that smaller pores are formed when removing the PPP.

The porosity in the films is then generated by removing the PPP by washing the dense films using an adequate solvent. The aramid is insoluble both in water and acetone, so the integrity of the film is guaranteed. In contrast, the minimum swelling (26% and 10% in water and acetone, respectively) of the aramid in these solvents allows their penetration into the film to remove the porosity promoters. The formation of the porous structure in the films can then be evidenced visually through the increase in the opacity of the films (see the photographs of the films after PPP removal in the Section S4 and Figure S6, together with AFM images of the film's

surface). However, to test both the washing efficiency and the optimal washing time, we performed washing tests using distilled water at 80°C for PA-PVA10 and PA-PEOx100 or acetone in a Soxhlet extractor for PA-CA50 for different periods (1.5, 3, 4.5, 6 and 8 h, until constant weight). For example, for PA-PVA10, most of the PVA is removed in the first hour, and no further removal is observed after 6 h (constant weight), and for PA-PEOx100, the film's weight is constant after washing for 3 h. In the case of CA removal, PA-CA50 weight is stable after extracting for 12 h with acetone. For that reason, we decided to wash the films containing PVA or PEOx for 12 h in water at 80°C, and the ones having CA using acetone in a Soxhlet extractor for 24 h. However, the PPP is not removed completely. We observed that neither by increasing the washing temperature using a pressure flask (150°C) nor by the increase in the washing time (48 h), further removal of the PPP is reached, evidenced in the constant weight of the samples and TGA thermograms. The presence of PPP in the washed films was evidenced using ¹H NMR (see Section S6 and Figure S8). We believe that the interactions (hydrogen bonds mainly) of the PPP with the PA prevent the PPP from being entirely removed from the film. To characterize this, we used FTIR spectroscopy. The broadening of the bands corresponding to the C=O stretching, and the N-H bending (1649 and 1605 cm^{-1} , respectively) is indicative

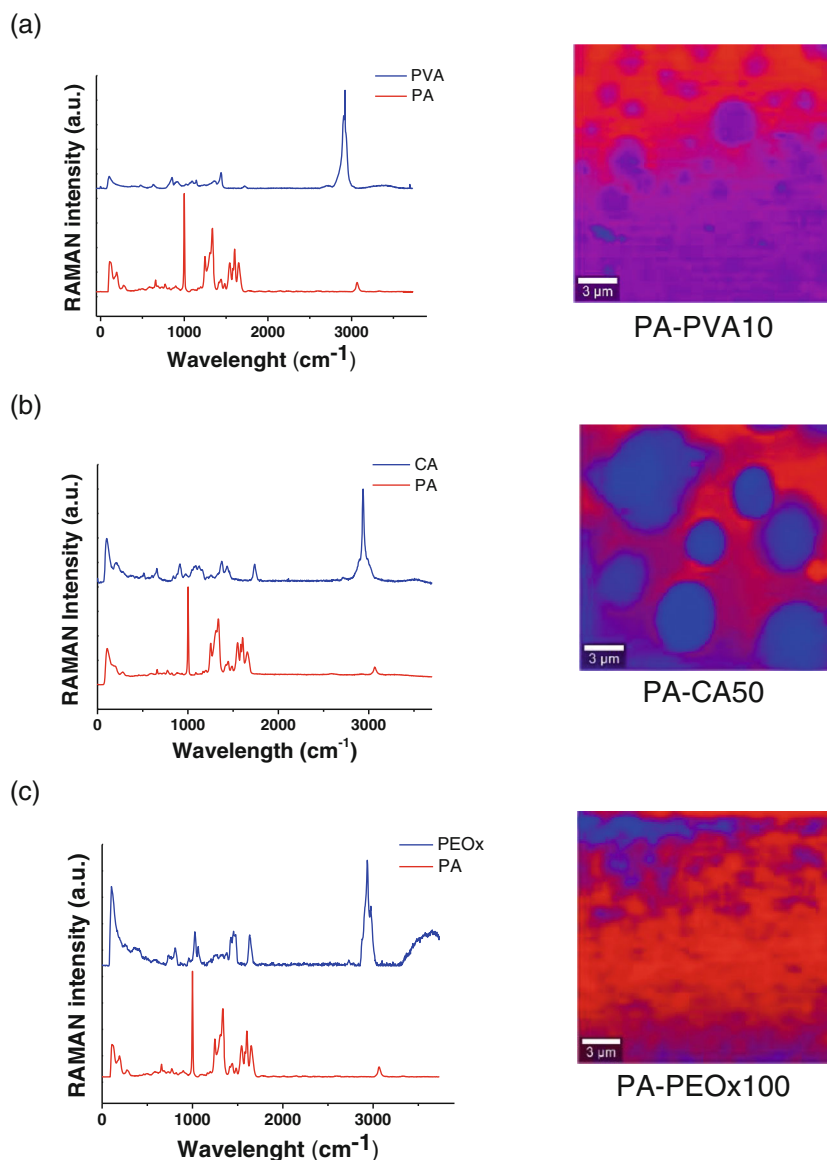


FIGURE 1 Raman and atomic force microscopy-Raman spectra collected for the single components (PA, CA, PEOx, and PVA), and their distribution along (a) PA-PVA10, (b) PA-CA50, and (c) PA-PEOx100 films [Color figure can be viewed at wileyonlinelibrary.com]

of the hydrogen bonding interaction of the PA with the PPP. This fact is especially evident when using PEOx since it is present in larger proportions, and these two bands are combined into one at 1607 cm^{-1} (Section S7 and Figure S9).

The porous structure and the mechanical and thermal properties of the films prepared this way with different porosity promoters and loading percentages were evaluated and compared to dense films prepared in the same manner. Furthermore, since the preparation of the films is carried out at a laboratory scale, the films' reproducibility and porosity, morphological parameters, and properties were also tested. For that purpose, we fabricated three replicates of some of the films (PA-PVA10-P and PA-PEOx100-P; see Section S1) and compared their properties, evidencing that the results were homogeneous and

concluding that our preparation method is adequate and reproducible.

3.2 | Morphological parameters and density

SEM micrographs of the surface and cross-section of the films after removing the porosity promoter (renamed by adding “-P” after the name of the film) were taken according to the procedure described in Section 2.2. To determine and characterize the porous structure. A uniform porous structure can be observed throughout the thickness of the films (see Section S2). Figure 2 shows the micrographs of the cross-section of the films at $\times 3000$ after removing the porosity promoters, and Table 3

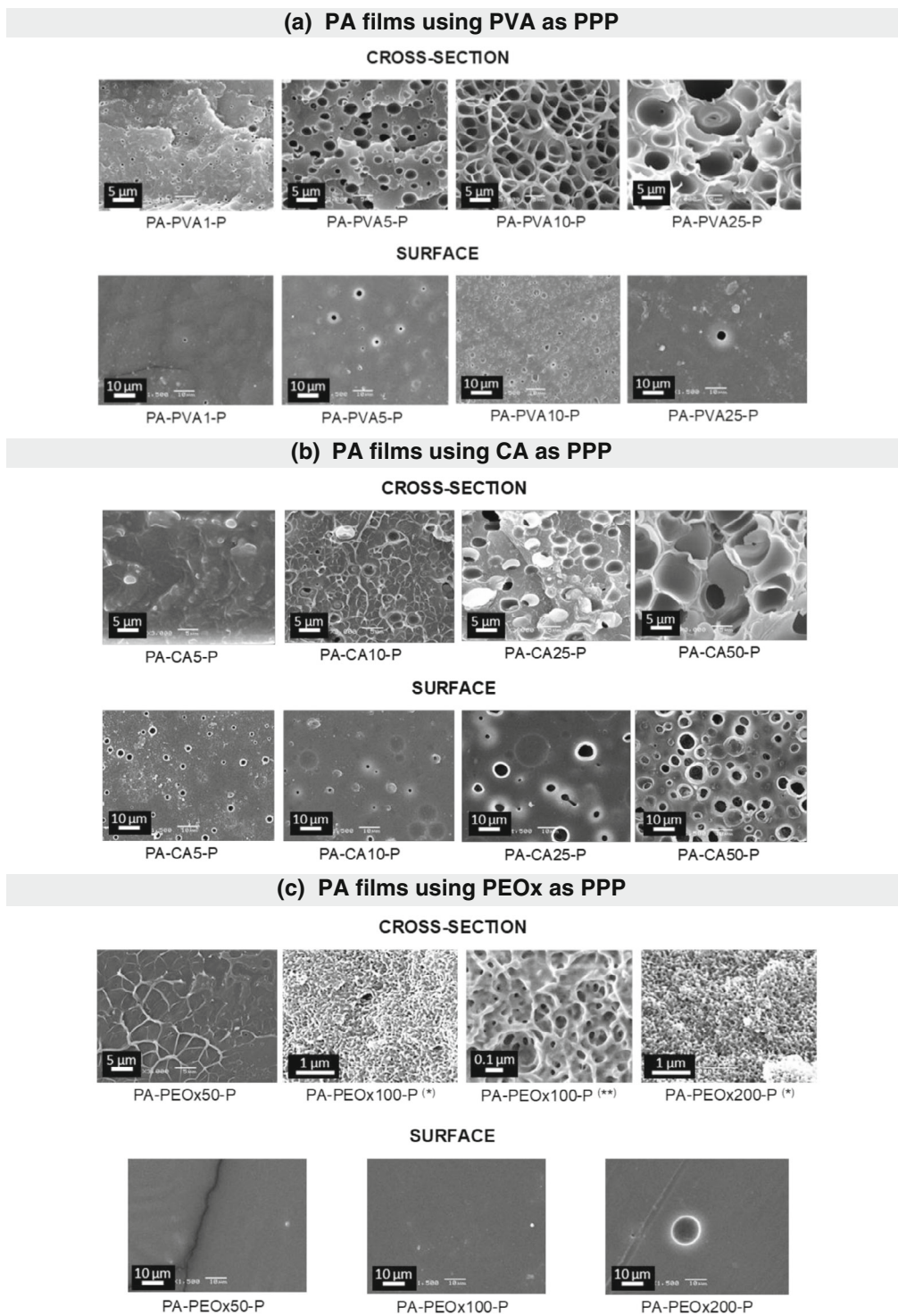


FIGURE 2 SEM micrographs of cross-section ($\times 3000$ magnification) and surface ($\times 1500$ magnification) of films prepared from PA and (a) PVA, (b) CA, and (c) PEOx in different proportions after removing the porosity promoter. *Cross-section SEM micrographs of PA-PEOx100-P and PA-PEOx200-P were taken at $\times 25,000$. Cross-section SEM micrograph of PA-PEOx100-P taken at $\times 100,000$ using a ZEISS GeminiSEM 560 equipment

summarizes the study of the observed structures using ImageJ software.

All the films prepared using PVA as the PPP (Figure 2a) showed a closed-pore structure, exhibiting

increasing pore sizes with the amount of PVA used. As observed in the cross-section, a very homogeneous and opened-cell porous structure is obtained for PA-PVA10-P. Although we expected the film fabricated using 25% of

TABLE 3 Comparative study of the porosity in films

| Polymer | Cross-section porosity | \bar{R} (μm) | Surface porosity | \bar{R} (μm) | Porous film density (g/cm^3) | Density reduction ^a (%) |
|--------------|------------------------|-----------------------------|------------------|-----------------------------|--|------------------------------------|
| PA | - | - | - | - | 1.42 (dense) | - |
| PA-PVA1-P | Very disperse | 1 | NO | | 1.26 | 11 |
| PA-PVA5-P | Disperse | 2–3 | Very disperse | 2 | 1.01 | 29 |
| PA-PVA10-P | Homogeneous | 2 | Homogeneous | 2–3 | 0.45 | 68 |
| PA-PVA25-P | Homogeneous | 5–7 | NO | | 0.53 | 63 |
| PA-CA1-P | NO | | NO | | 1.38 | 3 |
| PA-CA5-P | Clogged pores | 1 | Disperse | 1 | 1.20 | 15 |
| PA-CA10-P | Clogged pores | 2 | Disperse | 2 | 1.08 | 24 |
| PA-CA25-P | Clogged pores | 4–5 | Disperse | 4 | 0.9 | 37 |
| PA-CA50-P | Homogeneous | 8–10 | Homogeneous | 9–10 | 0.62 | 56 |
| PA-PEOx1-P | No pore generation | 1.41 | 1 | | | |
| PA-PEOx5-P | | 1.38 | 3 | | | |
| PA-PEOx10-P | | 1.29 | 9 | | | |
| PA-PEOx25-P | | 1.25 | 12 | | | |
| PA-PEOx50-P | | 1.38 | 3 | | | |
| PA-PEOx100-P | Homogeneous | 0.1–0.02 | NO | | 0.81 | 43 |
| PA-PEOx200-P | Homogeneous | 0.1–0.02 | NO | | 0.60 | 58 |

^aCompared to dense PA film.

PVA (PA-PVA25-P) to follow this trend, the obtained structure is irregular and shows diverse pore morphologies. This fact could be attributed to the solubility of PVA in the mixture PA-DMA-LiCl, which might be reaching its limit at 25% amount. Looking at the surface images, the only PVA proportion that renders homogeneous superficial porosity is the one prepared using 10% of PVA (PA-PVA10-P). This way, we can conclude that the ideal amount of PVA when using this PPP for the preparation of films to render a homogeneous cellular structure both in the cross-section and in the surface is 10%, with an average pore size of 2 μm in the cross-section and 2–3 μm in the surface of the films (Table 3).

SEM micrographs of the films prepared using CA as PPP (Figure 2b) showed that dispersed pores start to show up when using 5% of CA and their number and sizes increase with increasing CA percentage. However, most pores were clogged for loading percentages between 5% and 25% by sphere-like CA aggregates,³⁰ which is evidenced in the PA-CA25-P image. On the other hand, 50% CA loading renders films with a heterogeneous structure with pore sizes between 8 and 10 μm (Table 3). The surface of these films presents dispersed pores up to a 25% CA loading, while a 50% of CA generates a greater number of pores with sizes between 9 and 10 μm and a homogeneous superficial structure in the films. Since we know that the PPP is not entirely removed from the films, and

PA-CA50-P shows a porous structure on the surface, using AFM-RAMAN spectroscopy (Section S5 and Figure S7) we observed that the remaining CA is located covering the walls of the pores of the PA film. In this surface contact area, hydrogen bonds interactions between the two polymers take place.

As observed in the SEM micrographs, the preparation of films using PEOx as PPP (Figure 2c) with loading percentages lower than 100% resulted in dense films. Only high loading percentages (100% or 200%) rendered films with nanocellular and highly homogeneous structures, with relatively small pore sizes, between 0.02 and 0.1 μm , many orders of magnitude lower than in the films prepared using PVA and CA as PPP. Due to their chemical structure and nature, such small pore sizes and homogeneous distribution could be attributed to the high compatibility of PEOx with the aramid. However, surface porosity is not observed in any film (or very dispersed), including the 100% and 200% PEOx loaded films. In Table 3, a comparative study using ImageJ software of the pores observed in the SEM micrographs is described.

According to the density measurements, when PVA is used as PPP, the optimal amount to obtain a regular porous structure with density reduction is 10%, leading to a density reduction of 65%. For films where CA and PEOx were used, the highest density reduction (around 50%) is obtained when 50% and 200% of PPP are used,

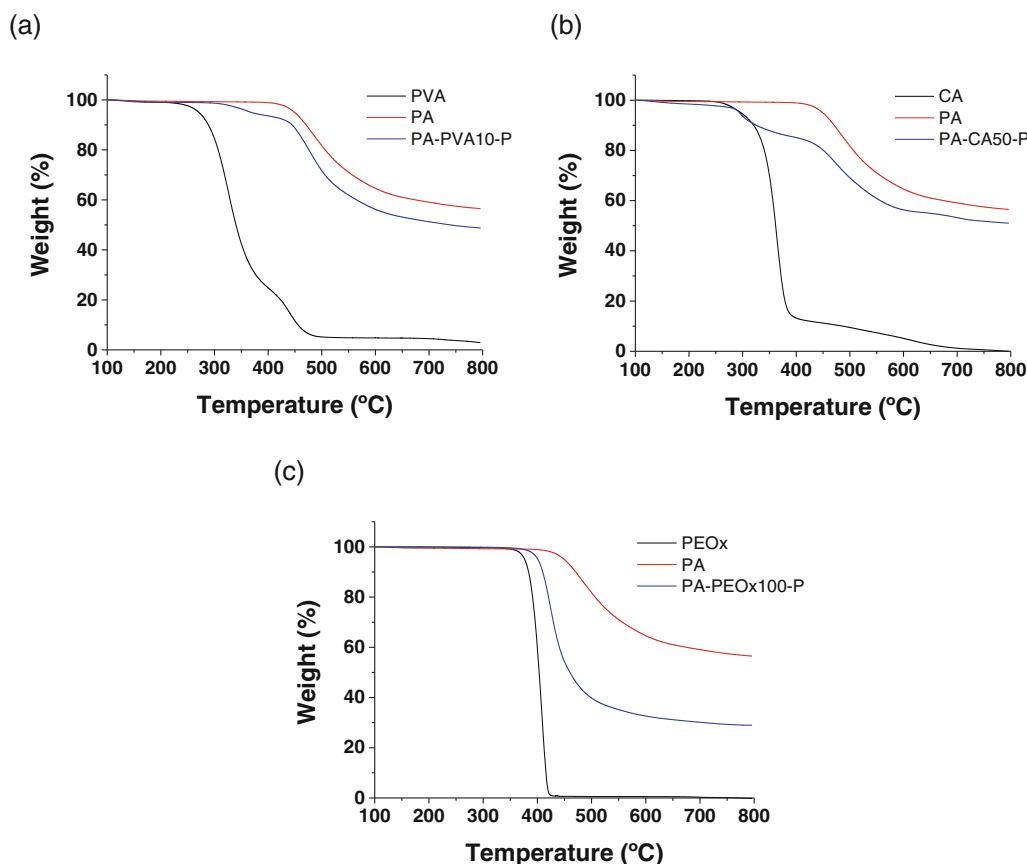


FIGURE 3 TGA curves under a nitrogen atmosphere obtained for the films prepared using different porosity promoter polymer (PPP) before and after removing the PPP and compared with the PA film and the corresponding PPP (a) PVA, (b) CA and (c) PEOx [Color figure can be viewed at wileyonlinelibrary.com]

respectively. However, a 200% PEOx content renders films with poor mechanical properties, so we considered 100% PEOx content as the optimal amount for films containing this PPP. For these reasons, from now on, some of the assays will only be performed for PA-PVA10, PA-CA50, and PA-PEOx100 films. These results show the efficiency in the density reduction compared to pure PA film, making these materials even lighter.

3.3 | Thermal performance

Thermogravimetric analyses were performed to evaluate the thermal properties of the films regarding their thermal resistance and to confirm the presence of the PPP or the washing procedure to obtain porous films.

Figure 3 shows the thermograms in nitrogen atmosphere of both the dense and porous films obtained using the optimal percentage for each PPP (10, 50, and 100 for PVA, CA, and PEOx, respectively), and they are compared to a washed PA film prepared in the same conditions, and to the corresponding PPP. Also, the thermograms obtained for the same films but using an

oxidizing atmosphere (Figure S6) can be found in Section S4. PA has outstanding thermal resistance, starting its degradation at nearly 500°C, very different from the thermal resistance of the rest of the polymers used, which begin their degradation at around 300–360°C.^{45–48}

When PVA is removed from the initial film, the temperature degradation curve resembles the one for the plain PA film (Figure 3a). However, a slight difference is still observed starting a 350°C due to PVA residues present in the PA-PVA10-P film. Regarding the films prepared using PEOx and CA, the removal of the PPP is not so efficient, as observed in Figure 3b,c. The fact that the degradation of the PPP inside the film starts at a higher temperature than the isolated PPP is indicative of an interaction between the PPP and the aramid.

DSC analyses were performed using the same samples as the thermogravimetric analysis (Figure 4). PVA (Figure 4a), as a semicrystalline polymer, shows two transitions, a glass transition (T_g) at 72°C and a melting temperature (T_m) at 170°C.⁴⁹ PA films show a T_g of 281°C, and for the film PA-PVA10-P, a transition at around 170°C shows up, and a slight lowering of the T_g of the aramid, due to PVA residues present.

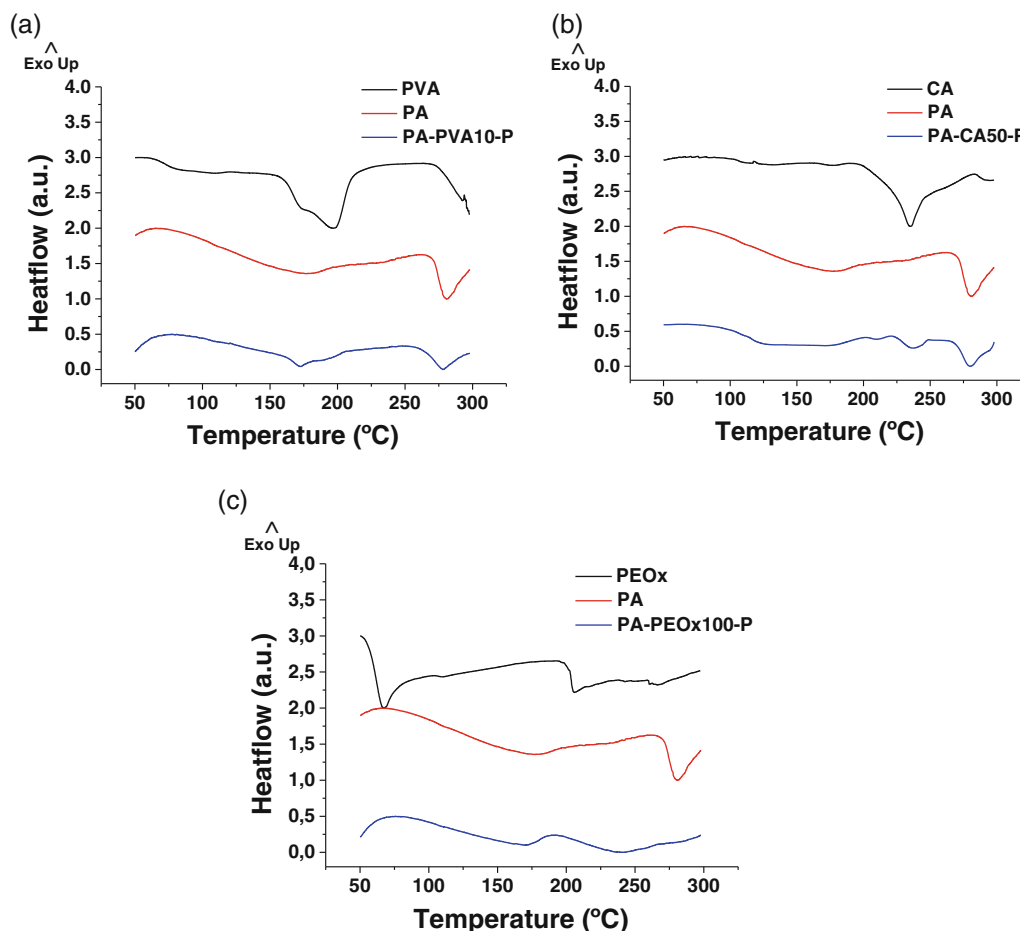


FIGURE 4 Differential scanning calorimetry curves of the films prepared using different porosity promoter polymer (PPP) after removing the PPP and compared with the PA film and the corresponding PPP (a) PVA, (b) CA, and (c) PEOx [Color figure can be viewed at wileyonlinelibrary.com]

CA shows a melting temperature of 235°C.⁵⁰ This time, the DSC curve of the film after washing the PPP (Figure 4b) does not match the curve of the PA film due to the presence of the PPP in a higher proportion. The same phenomenon is observed for PA-PEOx100-P DSC curves, showing the presence of PEOx, and even not observing the T_g of the PA after washing.

The thermal conductivity between the two surfaces of PA, PA-PVA10-P and PA-PEOx100-P films was measured to see the influence of the pore size in the thermal insulation of the materials. The results showed that PA film thermal conductivity was 0.02575 ± 0.00008 W/mK. This value was reduced to the half for PA-PEOx100-P film (0.01242 ± 0.00002 W/mK) with pore sizes between 0.02 and 0.1 μm . The thermal conductivity value of PA-PVA10P films was found to be between these two values (0.02142 ± 0.00004 W/mK), showing pore sizes of around 2 μm . This fact demonstrates the Knudsen effect, since the thermal conductivity decreases with increasing pore sizes. This effect takes place when the cell size is

comparable or lower than the free path of the gas molecules (air) contained in the material.⁵¹

3.4 | Mechanical performance

The mechanical parameters obtained from the traction assays of the porous films prepared using different proportions of PPP are summarized in Table 4. In order to compare the properties of the films with each other, the averaged values of the mechanical parameters are divided by the density of each film (E_r , relative Young's moduli and σ_r^{bp} is the relative tensile strength).

For the films prepared using PVA as the PPP, both the relative Young's Modulus and tensile strength increase with the film porosity, demonstrating the positive effect of the cellular structure on the material's rigidity. This way, PA-PVA10-P is 50% stiffer than a PA film. Also, the tensile strength is optimum for the film prepared using 10% of PVA, having a homogeneous and

TABLE 4 Relative mechanical properties of each film after porosity promoter polymer removal. E_r , relative Young's moduli and σ_r^{bp} is the relative tensile strength

| Film | E_r (MPa) ^a | σ_r^{bp} (MPa) ^a |
|--------------|--------------------------|------------------------------------|
| PA (dense) | 1001 ± 56 | 57 ± 9 |
| PA-PVA1-P | 915 ± 53 | 43 ± 2 |
| PA-PVA5-P | 1362 ± 63 | 76 ± 2 |
| PA-PVA10-P | 1570 ± 97 | 143 ± 7 |
| PA-PVA25-P | 1632 ± 65 | 92 ± 2 |
| PA-CA5-P | 1335 ± 94 | 84 ± 2 |
| PA-CA10-P | 1286 ± 17 | 64 ± 1 |
| PA-CA25-P | 1133 ± 36 | 64 ± 2 |
| PA-CA50-P | 538 ± 81 | 54 ± 2 |
| PA-PEOx100-P | 480 ± 64 | 42 ± 15 |
| PA-PEOx200-P | 618 ± 47 | 44 ± 13 |

^aRelative values. The averaged mechanical parameters are divided by the density of the film for comparison purposes.

open-cell porous structure. At the same time, PA-PVA25-P starts showing a decrease in tensile strength, probably due to the increase in the pore radius. The mechanical properties of PA-CA1-P film were not measured since it does not show a porous structure. For low percentages of CA used in the preparation of the films, the relative Young's moduli increase compared to dense PA. However, a decrease of the Young's Modulus is observed with the increasing amount of CA. The high modulus of the films is attributed to the rigid structure of *m*-aramid, and the presence of unwashed CA should decrease the mechanical performance of the films unless new interactions (hydrogen bonding) are formed between the components. However, with increasing amounts of CA, the positive effect of the interactions between the two polymers is counteracted by the lower mechanical performance of the CA. PA-CA50-P shows a lower Young's modulus than neat PA film, which can be attributed to the presence of macrovoids and cavities and a heterogeneous porous structure. The tensile strength is diminished with increasing amounts of PPP and porosity, making the films more brittle but comparable to neat PA films. The use of PEOx as the PPP renders less-stiff films with lower Young's moduli and similar tensile strength than neat PA films. Since the amount of PEOx still present after washing the film is noticeable, a plasticization of the films is observed.

4 | CONCLUSIONS

In short, we were able to obtain porous aramid films by using three different compatible polymers (PVA, CA, and

PEOX) in different proportions, which generated a porous structure after their removal in distilled water or acetone. Different pore sizes and morphologies can be obtained this way, varying from closed-pore to opened-cell structures, ranging from 0.02 to 10 μm. Also, pores can be found only in the cross-section or both in the cross-section and the surface of the films, with a density reduction of up to 65% compared to commercial poly (*m*-phenylene isophthalamide). The removal of the porosity promoters was tested, and although the PPP is not entirely removed in all the cases, a porous structure is still observed. The mechanical performance of the films is related to the pore size and morphology generated, obtaining, for example, a 30% increase in the Young's Modulus for PA-PVA10-P film compared to a dense PA film. This way, the use of 10% of PVA in the film formulation as porosity former and later removal allows the reduction of commercial *m*-aramid's density without impairing its thermal performance and even improving the relative mechanical behavior. Low-density high-performance polymers development is crucial to reducing fuel consumption, considering the current global energy crisis. Moreover, porous polymers are gaining interest in the scientific community since cavities can locate different types of molecules, providing them potential applications in energy storage, gas separation or catalysis, aeronautics, renewable energies, automotive, construction, or biotechnology, among others. This work opens the possibility to explore further this methodology of preparing porous films, through the proper selection of the porosity promoter (or a combination of more than one) and the proportions used in order to obtain the controlled pore distribution and morphology that better suits the final requirements of the material.

AUTHOR CONTRIBUTIONS

Miriam Trigo-López: Conceptualization (lead); formal analysis (equal); investigation (lead); methodology (lead); project administration (lead); supervision (equal); validation (equal); writing – original draft (lead). **Andrea Rubio Aguinaga:** Data curation (equal); formal analysis (equal); methodology (equal); writing – original draft (equal). **José Antonio Reglero Ruiz:** Conceptualization (equal); data curation (lead); formal analysis (equal); supervision (equal); writing – review and editing (equal). **María Asunción Muñoz Santamaría:** Formal analysis (supporting); supervision (equal); writing – review and editing (equal). **Félix C. García García:** Conceptualization (equal); investigation (equal); project administration (equal); writing – review and editing (equal). **José Miguel García Pérez:** Conceptualization (equal); investigation (equal); supervision (equal); validation (equal); writing – original draft (equal).

ACKNOWLEDGMENT

The authors gratefully acknowledge the financial support provided by the Regional Government of Castilla y León (Junta de Castilla y León), the Ministry of Science and Innovation MICIN and the European Union NextGenerationEU / PRTR, and the Spanish Agencia Estatal de Investigación (State Research Agency) (PID2019-108583RJ-I00/AEI/10.13039/501100011033).

CONFLICT OF INTEREST

The authors declare no conflict of interest.

DATA AVAILABILITY STATEMENT

The raw/processed data required to reproduce these findings cannot be shared at this time as the data also forms part of an ongoing study.

ORCID


Andrea Rubio-Aguinaga  <https://orcid.org/0000-0003-1144-8970>

José Antonio Reglero-Ruiz  <https://orcid.org/0000-0002-7075-3206>

Asunción Muñoz  <https://orcid.org/0000-0002-0063-3057>

Félix C. García  <https://orcid.org/0000-0002-1784-6884>

José M. García  <https://orcid.org/0000-0002-2674-8194>

Miriam Trigo-López  <https://orcid.org/0000-0001-5948-1230>

REFERENCES

- [1] J. Wu, F. Xu, S. Li, P. Ma, X. Zhang, Q. Liu, R. Fu, D. Wu, *Adv. Mater.* **2019**, *31*, 1802922.
- [2] D. Wu, F. Xu, B. Sun, R. Fu, H. He, K. Matyjaszewski, *Chem. Rev.* **2012**, *112*, 3959.
- [3] Q. Shilun, T. Ben, *Porous Polymers: Design, Synthesis and Applications*, Royal Society of Chemistry, Cambridge **2016**. <https://doi.org/10.1039/9781782622260>
- [4] J. Huang, X. Zhou, A. Lamprou, F. Maya, F. Svec, S. R. Turner, *Chem. Mater.* **2015**, *27*, 7388.
- [5] Y. Hoshino, Y. Arata, Y. Yonamine, S.-H. Lee, A. Yamasaki, R. Tsuchiura, K. Yano, K. J. Shea, Y. Miura, *Polym. J.* **2015**, *47*, 220.
- [6] T. Malik, H. Razzaq, S. Razzaque, H. Nawaz, A. Siddiq, M. Siddiq, S. Qaisar, *Polym. Bull.* **2019**, *76*, 4879.
- [7] S. Remanan, M. Sharma, S. Bose, N. C. Das, *ChemistrySelect* **2018**, *3*, 609.
- [8] A. Venault, Y. Chang, D.-M. Wang, D. Bouyer, *Polym. Rev.* **2013**, *53*, 568.
- [9] G. R. Guillen, Y. Pan, M. Li, E. M. V. Hoek, *Ind. Eng. Chem. Res.* **2011**, *50*, 3798.
- [10] D. R. Lloyd, K. E. Kinzer, H. S. Tseng, *J. Memb. Sci.* **1990**, *52*, 239.
- [11] D. R. Lloyd, S. S. Kim, K. E. Kinzer, *J. Memb. Sci.* **1991**, *64*, 1.
- [12] L. Vogelaar, J. N. Barsema, C. J. M. van Rijn, W. Nijdam, M. Wessling, *Adv. Mater.* **2003**, *15*, 1385.
- [13] F. E. Ahmed, B. S. Lalia, R. Hashaikeh, *Desalination* **2015**, *356*, 15.
- [14] J.-J. Kim, T.-S. Jang, Y.-D. Kwon, U. Y. Kim, S. S. Kim, *J. Memb. Sci.* **1994**, *93*, 209.
- [15] P. Apel, *Radiat. Meas.* **2001**, *34*, 559.
- [16] Y. S. Kim, K. Y. Suh, H. H. Lee, *Appl. Phys. Lett.* **2001**, *79*, 2285.
- [17] B. G. Thiam, A. El Magri, H. R. Vanaei, S. Vaudreuil, *Polymers (Basel)*. **2022**, *14*, 1023.
- [18] J. A. Reglero Ruiz, M. Trigo-López, F. C. García, J. M. García, *Polymers (Basel)*. **2017**, *9*, 414.
- [19] B. S. Pascual, M. Trigo-López, C. Ramos, M. T. Sanz, J. L. Pablos, F. C. García, J. A. Reglero Ruiz, J. M. García, *Eur. Polym. J.* **2019**, *110*, 9.
- [20] M. Haurat, M. Dumon, *Molecules* **2020**, *25*, 5320.
- [21] B. S. Pascual, M. Trigo-López, J. A. Reglero Ruiz, J. L. Pablos, J. C. Bertolin, C. Represa, J. V. Cuevas, F. C. García, J. M. García, *Eur. Polym. J.* **2019**, *116*, 91.
- [22] M. Trigo-López, S. Vallejos, J. A. Reglero Ruiz, A. García-Gómez, M. Seara-Martínez, F. C. García, J. M. García, *Polymer (Guildf)*. **2020**, *202*, 122629.
- [23] S. Dewilde, W. Dehaen, K. Binnemans, *Green Chem.* **2016**, *18*, 1639.
- [24] S. Dewilde, T. Vander Hoogerstraete, W. Dehaen, K. Binnemans, *Chem. Eng.* **2018**, *6*, 1362.
- [25] Y. Cao, Y. Chen, X. Sun, Z. Zhang, T. Mu, *Phys. Chem. Chem. Phys.* **2012**, *14*, 12252.
- [26] E. A. Chernikova, L. M. Glukhov, V. G. Krasovskiy, L. M. Kustov, M. G. Vorobyeva, A. A. Koroteev, *Russ. Chem. Rev.* **2015**, *84*, 875.
- [27] L. Miao, Y. Wu, J. Hu, P. Wang, G. Liu, S. Lin, Y. Tu, *J. Memb. Sci.* **2019**, *578*, 16.
- [28] T. X. Viegas, M. D. Bentley, J. M. Harris, Z. Fang, K. Yoon, B. Dizman, R. Weimer, A. Mero, G. Pasut, F. M. Veronese, *Bioconjugate Chem.* **2011**, *22*, 976.
- [29] A. Shubha, S. R. Manohara, *J. Polym. Res.* **2018**, *25*, 174.
- [30] S. Fischer, K. Thümmel, B. Volkert, K. Hettrich, I. Schmidt, K. Fischer, *Macromol. Symp.* **2008**, *262*, 89.
- [31] A. H. Bahmanpour, T. Navaei, F. Ahadi, in *Handbook of Biomaterials Biocompatibility*, Woodhead Publishing, Sawston, United Kingdom **2020**, p. 653. <https://doi.org/10.1016/B978-0-08-102967-1.00029-3>
- [32] M. Chanda, *Plastics Technology Handbook*, Fifth ed., CRC Press, New York **2017**. <https://doi.org/10.1201/9781315155876>
- [33] P. Song, Z. Xu, Y. Lu, Q. Guo, *Macromolecules* **2015**, *48*, 3957.
- [34] L. Yao, C. Lee, J. Kim, *Fibers Polym.* **2011**, *12*, 197.
- [35] N. E. Putra, A. Tigrine, S. Aksakal, V. R. de la Rosa, P. Taheri, L. E. Fratila-Apachitei, J. M. C. Mol, J. Zhou, A. A. Zadpoor, *Mater. Sci. Eng. C* **2021**, *133*, 112617.
- [36] S. Hashimoto, M. Morishita, T. Sakai, *EP* **2022**, *A1*, 4020694.
- [37] M. H. Parekh, S. Oka, J. Lutkenhaus, V. G. Pol, *ACS Appl. Mater. Interfaces* **2022**, *14*, 29176.
- [38] J. H. Lee, J. Manuel, Y. Liu, K. E. Park, W. H. Park, J.-H. Ahn, *J. Nanosci. Nanotechnol.* **2016**, *16*, 10724.
- [39] S. Qingjin, H. Heji, L. Wei, L. Xiang, Aromatic polyamide porous membrane, method for preparing, and lithium secondary battery having the same, 20190074500, 2019.
- [40] M. Trigo López, J. A. Reglero Ruiz, J. L. Pablos, D. E. Ciurduc, T. Corrales, F. C. García, J. M. García, *J. Photochem. Photobiol., A* **2022**, *422*, 113571.

- [41] Z. Zhang, L. He, C. Zhu, Y. Qian, L. Wen, L. Jiang, *Nat. Commun.* **2020**, *11*, 875.
- [42] H. Yan, X. Miao, J. Xu, G. Pan, Y. Zhang, Y. Shi, M. Guo, Y. Liu, *J. Memb. Sci.* **2015**, *475*, 504.
- [43] R. Revanur, I. Roh, J. E. Klare, A. Noy, O. Bakajin, Thin film composite membranes for forward osmosis, and their preparation methods, US 8920654B2, **2014**.
- [44] L. Oliveira-Salmazo, A. Lopez-Gil, F. Silva-Bellucci, A. E. Job, M. A. Rodriguez-Perez, *Ind. Crops Prod.* **2016**, *80*, 26.
- [45] M. K. Ozturk, B. Nergis, C. Candan, *IOP Conf. Ser. Mater. Sci. Eng.* **2018**, *460*, 012048.
- [46] N. A. Betti, *Eng. Technol. J.* **2016**, *34*, 2433.
- [47] M. da Conceição, C. Lucena, A. E. V. de Alencar, S. E. Mazzeto, S. de Soares, *Polym. Degrad. Stab.* **2003**, *80*, 149.
- [48] N. Oleszko-Torbus, A. Utrata-Wesołek, M. Bochenek, D. Lipowska-Kur, A. Dworak, W. Walach, *Polym. Chem.* **2020**, *11*, 15.
- [49] P. Liu, W. Chen, C. Liu, M. Tian, P. Liu, *Sci. Rep.* **2019**, *9*, 9534.
- [50] M. de Carvalho Eufrásio, D. D. Pinto, A. L. da Silva, V. dos Amorim Gomes, S. A. Leite, A. R. Fialho e Moraes, R. F. de Novais, J. Tronto, F. G. Pinto, *RSC Adv.* **2019**, *9*, 5620.
- [51] B. Notario, J. Pinto, E. Solorzano, J. A. de Saja, M. Dumon, M. A. Rodríguez-Pérez, *Polymer (Guildf)*. **2015**, *56*, 57.

SUPPORTING INFORMATION

Additional supporting information can be found online in the Supporting Information section at the end of this article.

How to cite this article: A. Rubio-Aguinaga, J. A. Reglero-Ruiz, A. Muñoz, F. C. García, J. M. García, M. Trigo-López, *J. Appl. Polym. Sci.* **2022**, *139*(47), e53192. <https://doi.org/10.1002/app.53192>